PCCP

Optimizing the Orbital Occupation in the Multiple Minima Problem of Magnetic Materials from the Metaheuristic Firefly Algorithm

Journal:	*Physical Chemistry Chemical Physics*
Manuscript ID	CP-ART-06-2019-003618.R2
Article Type:	Paper
Date Submitted by the Author:	05-Sep-2019
Complete List of Authors:	Payne, Adam; West Virginia University, Physics and Astronomy Avendaño-Franco, Guillermo; West Virginia University, Physics and Astronomy He, Xu; Liege University, Institu de Physique Bousquet, Eric; University of California Santa Barbara CA , Materials Department; Liege University, Institu de Physique Romero, Aldo; West Virginia University, Physics and Astronomy

PCCP

ARTICLE TYPE

Cite this: DOI: 00.0000/xxxxxxxxxx

Optimizing the Orbital Occupation in the Multiple Minima Problem of Magnetic Materials from the Metaheuristic Firefly Algorithm

Adam Payne,[a], Guillermo Avedaño-Franco,[b], Xu He[c], Eric Bousquet[c] and Aldo H. Romero[b]

Received Date
Accepted Date

DOI: 00.0000/xxxxxxxxxx

We present the use and implementation of the firefly algorithm to help in scanning the multiple metastable minima of orbital occupations in Density Functional Theory (DFT) plus Hubbard U correction and to identify the ground state occupations in strongly correlated materials. We show the application of this implementation with the Abinit code on $KCoF_3$ and UO_2 crystals, which are typical d and f electron systems with numerous occupation minima. We demonstrate the validity and performance of the method by comparing with previous methodologies. The method is general and can be applied to any code using constrained occupation matrices.

1 Introduction

The two most widely used approximations for exchange-correlation potential in density functional theory (DFT), the local density approximation (LDA) and the generalized gradient approximation (GGA), fail to capture the electronic structure of materials where partially filled d and f-electrons are at play.[1,2] This particular failure comes from the tendency of LDA/GGA to delocalize electrons due to the presence of self-interaction. Several methods have been developed to correct this problem, e.g. the self-interaction correction (SIC)[3–6], the inclusion of Hubbard U repulsion into the DFT Hamiltonian for some selected orbitals[7], hybrid-functionals[7–9] or dynamical mean-field theory (DFT+DMFT)[10–13]. Among them, the DFT+U method is the most widely used because of its simple scheme and its ease of use, it does not cost much more simulation time than a regular LDA/GGA calculation (contrary to the other methods). However, this correction also allows the presence of many metastable occupation states for the orbitals corrected with the Hubbard U parameter[14–17] (the same problem is also present for hybrid functionals or Hartree-Fock methods). The presence of these numerous metastable states makes the usual self-consistent algorithms to solve the DFT equation, such as the conjugate gradient algorithm, to fail in finding the orbital occupation that gives the global energy minimum of the system. If a calculation starts with an initial occupation which is close to one local minimum, it could converge towards this metastable state without exploring the other possibilities even though they are at lower energy. The other way around, in some cases these metastable states are close enough in energy to let the minimization algorithm to jump from one to the other but without the guaranty that the final reached state is the ground state.

One solution would be to sample the configuration space of all the allowed possible occupancies of the system such that the lowest energy orbital configuration can be found. Quasi-annealing, dynamical mean-field theory (DMFT) and occupation matrix control have been used to solve this problem, but each has its drawbacks. In quasi-annealing, a fictitious fluctuation of the external potential is applied and gradually suppressed to reach the correct ground state. This method is analogous to gradually annealing the thermal kinetic energy in a classical system to reach a local minimum. This provides to a case stuck in a minimum to gain enough energy to overcome the barrier between it and another minimum. The main drawback of this method is that it struggles with locating the correct ground state in systems with many minima which are close in the calculated energy and width around this[18]. DMFT consists of mapping the many-body lattice model, for example, the Hubbard model, to a local quantum impurity model, in this case, the Anderson impurity model, and subjects this to a self-consistency condition. Effectively, DMFT finds the Green's function for the impurity model which also reproduces the lattice model's Green's function through the interaction with an effective mean field. While this is an alternative method to using DFT, it is computationally demanding[12,13].

In this paper we propose a new method to sample this configuration space based on the Firefly algorithm (FA)[19,20]. This method builds upon manipulating the occupation matrix, effectively exploring the configuration space of the problem, however,

[a]West Virginia University, Morgantown, WV 26505; E-mail: apayne9@mix.wvu.edu
[b]West Virginia University, Morgantown, WV 26505
[c]Physique Théorique des Matériaux, Q-MAT, CESAM, Université de Liége, B-4000 Sart Tilman, Belgium

the approach is not trivial and some caveats must be addressed.

The first is that the occupation control method necessitates the generation and testing of several initial occupancies. For a single unit cell with one atom, this is a fairly trivial task. For example, with an atom that requires d-electron corrections, there are at most $\frac{5!}{3!2!} = 10$ possible configurations. This becomes much more complex whenever there are multiple atoms, or when supercells must be constructed to fully capture correlation effects, such as in antiferromagnets. Instead of trying to determine all possible configurations by hand, FA selectively explores differing orbital configurations on the potential energy surface (PES) of possible orbital configurations. This will be described in further detail in the methodology section. We will apply this method to two test cases: the cubic perovskite $KCoF_3$, which requires 3-d electron corrections, and UO_2, which requires corrections to 5-f electrons.

The structure of the paper is as follows: First, the general methodology of FA will be described. Next, the computational details of its implementation are discussed. In the final two sections, the results of FA applied to $KCoF_3$ and UO_2 will be presented and discussed.

2 Methodology

The Firefly algorithm (FA) is a population-based metaheuristic which is inspired by the behavior of fireflies in nature [19,20]. As a population-based method, an initial population of candidate fireflies with randomized properties is first generated. To generate an initial random population of these candidates, which will be a collection of different orbital occupation matrices, we apply a unitary transformation to a fixed occupation matrix. This initial fixed matrix is determined by the number of electrons that are being corrected, in the sense of DFT+U, in a given material system; the trace of this matrix is equal to the total number of electrons. Since the application of a unitary transformation does not change the trace, the total number of electrons is not modified in the considered system. The unitary transformation matrices can be generated by defining a series of independent parameters, as presented in the work by Hoffman *et. al.*.[21] In general, any N-dimensional unitary transformation can be represented by $\frac{1}{2}N(N-1)$ independent parameters. In this work, the parameters have the following constraints:

$$\frac{-\pi}{2} < \theta_k < \frac{\pi}{2} \tag{1}$$

$$-\pi < \theta_{N-1} < \pi \tag{2}$$

$$\theta_N = \frac{\pi}{2} \tag{3}$$

, with $k = 1,2,3,...,N-2$.

In the case of $N = 3$, these are the ordinary Euler angles, so these are referred to as *generalized* Euler angles. In the case of d-orbitals, the occupation matrix is of 5x5 dimension, which means ten Euler angles must be generated. For f-orbitals, the occupation matrix is 7x7, so 21 Euler angles are required. Once this transformation is applied to the initial fixed occupation, a new point is reached in the orbital configuration space. A set of Euler angles are generated for every member of this initial population as they allow for the generation of differing initial occupations for each candidate. Each candidate is then evaluated for how optimal of a solution it is to some problem. How "bright" a candidate determines how optimal it is as a solution. And just as in nature, multiple spatial distributions of fireflies can have equivalent brightness, meaning that FA is multi-modal; it can both explore multiple regions of the PES and have multiple solutions with the same total energy. This is precisely why it is well-suited to searching for optimal orbital occupations; degenerate occupations are not uncommon. Fireflies are attracted to any region of brighter fireflies, and this attraction is modulated by the distance. This attraction is the rule for how the solution space is explored: As a candidate moves towards a more optimal candidate, its properties are modified to become more like the more optimal candidate. The following expression governs how each candidate firefly is modified towards more optimal candidates:

$$x_i^{t+1} = x_i^t + \sum_j \beta e^{-\gamma r_{ij}^2}(x_j^t - x_i^t) + \alpha_t \varepsilon_t \tag{4}$$

This expression governs how the ith candidate in generation t is updated to form candidate i in generation $t+1$. The first term on the right-hand side is the unmodified candidate in generation t. In our case, each candidate corresponds to a particular orbital occupation. The components of candidate i are modified from generation t to generation $t+1$ by every candidate configuration which is lower in energy, as total energies are our measure of "brightness". The term $\beta e^{-\gamma r_{ij}^2}$ defines the attractiveness of firefly i to firefly j. β defines the overall strength of attraction, since terms with $r_{ij} = 0$ evaluate to β. If $\beta = 0$, the searcher becomes a random walk. γ acts as a length scale, and controls the speed of convergence of the calculation. For the special case γ=0, candidate i finds all lower-energy candidates equally attractive, and the algorithm becomes a particle swarm. The last term adds randomness to the search, where ε_t is a vector with components that come from a random selection of a Gaussian distribution. α_t essentially controls the amount of randomness in the searcher. Once all candidates are moved, they checked against each other to ensure that none are equivalent. Ideally, by equivalent we mean they have the same orbital occupation, but from a numerical perspective, a tolerance must be introduced to define similarity. If any candidates are considered equivalent, the redundant candidates are replaced with random candidates. Similarity is defined in the same terms as the distance between candidates. In our case, physical distance is meaningless, as the points on our PES are differing orbital occupations. Since each point on the PES can be characterized by a unique set of Euler angles, the average difference between the angles can be used to define this distance. The functional form of this measure is displayed in Equation 5

$$r_{ij} = \frac{1}{N}\sum_k^N(\theta_i^k - \theta_j^k) \tag{5}$$

Here, N is the total number of Euler angles, θ_i^k is the kth Euler angle for candidate i, and θ_j^k is the kth Euler angle for candidate j. After this process, all of the moved candidates are promoted to the next generation along with the current lowest-energy solu-

tion. The process continues iteratively until a low-energy candidate survives for a specified number of generations. From previous work, ten generations provides an ideal compromise between accuracy and efficiency.

3 Computational Details

The ABINIT code[22–26] was used for all DFT calculations with the possibility to have both DFT+U and orbital occupation control.

The LDA/GGA functionals of DFT predict that $KCoF_3$ is metallic[27], which calls for a method to go beyond ordinary DFT. As discussed, we explored the performance of DFT+U as the method to correct the electron correlation in normal GGA functionals. As this is an antiferromagnet, it has 4 magnetic cations in the basic unit cell. This already creates a large set of possible energy minima states based on the different (U,J) parameters used in DFT+U. Since FA requires the calculation of multiple candidates simultaneously for at least ten generations, DFT+U appears the best option to efficiently test our FA's accuracy.

The initial occupancy remains fixed for 20 electronic self-consistent iterations. After these initial 20 iterations, the occupation matrix is allowed to relax, which causes it to converge to the nearest low-energy state. For $KCoF_3$, an energy cutoff of 708 eV and a k-point mesh of 4x4x4 was found to allow relaxation of the orbitals to a residual of the potential to a tolerance of 10^{-16}. The same tolerance was reached for UO_2 with an energy cutoff of 544 eV and a k-point grid of 2x8x8. Additionally, all calculations used the JTH v1.0 pseudopotentials with LDA exchange-correlation functionals.[28,29]. For Co, 17 valence electrons were considered, and for U 14 were considered. ABINIT allows for straightforward control of the occupancy matrices with the use of the dmatpawu variable.[26] For d-electron corrections, these are 5x5 matrices for each atom which requires d-orbital corrections using the DFT+U method, in particular Liechtenstein's rotational invariant method + FLL double-counting corrections[30,31]. For f-electron corrections, 7x7 matrices for each U atom are used. The initial values for these matrices were determined by considering the total number of electrons per corrected atom and defining diagonal matrices such that the trace of these matrices is equal to the total number of electrons in the f orbitals. FA handles the generation of new occupation matrices for each random candidate by selecting random Euler angles and applying the corresponding unitary transformation to each of these diagonal matrices. The implementation of FA in the PyChemia software package is used for performing all searches. A link to the GitHub repository for the package is contained in the reference.[32]

After a set of occupation matrices have been chosen to be the lowest energy, we have calculated the magnetic exchange couplings as a function of the U parameter. For each candidate $KCoF_3$ state, the magnetic exchange interaction parameters are calculated using the magnetic force theorem (MFT)[33], which use local spin rotation as a perturbation and calculate the response with Green's function method. To get the local perturbation, Maximally localized Wannier functions (MLWF) [34] for Co $3d$ and F $2p$ orbitals were constructed and the Kohn-Sham Hamiltonian from Abinit is mapped onto this basis set. Thus we can apply MFT to the Hamiltonian and get the exchange parameters[35].

4 Results

4.1 $KCoF_3$

The first system chosen to show the application of our FA implementation for orbital occupations is the cubic perovskite $KCoF_3$ with space group *Pm-3m*, an anti-ferromagnetic Mott insulator[36,37]. The cell parameters are $a = b = c = 4.105$Å. The Wyckoff positions for the cell used are listed in Table 1. A 2x2x2 supercell built from this unit cell is used for all calculations. This supercell is shown in Figure 1. The structures for both $KCoF_3$ and UO_2 are taken from the Materials Project.[38]

$KCoF_3$ *Pm-3m*

Atom	Wyckoff Position	x	y	z
K1	a	0.00	0.00	0.00
Co2	b	0.50	0.50	0.50
F1	3c	0.00	0.50	0.50

Table 1 Structural information for $KCoF_3$. Coordinates for each atom are in reduced coordinates.

The F atoms octahedron crystal field (CF) splits the Co 3d-orbitals into three degenerate t_{2g} (d_{xy}, d_{xz}, and d_{yz}) and two e_g degenerate orbitals ($d_{3z^2-r^2}$, and $d_{x^2-y^2}$)[39]. In general, for Co^{2+} in an octahedral crystal field, the CF splitting Δ is small, which yields the high-spin occupancy $t_{2g}^5 e_g^2$ with a nominal magnetic moment of $3\mu_B$. If Δ is large, the low-spin configuration is favored with the occupancy $t_{2g}^6 e_g^1$ and a nominal magnetic moment of $1\mu_B$. Experimentally, the magnetic moment of Co in $KCoF_3$ is 3.33 μ_B[39], which corresponds to the high-spin configuration, and its band gap is 2.1 ± 0.2 eV.[40] Table 2 lists the band gaps for the best candidates for each value of U and J considered. In regards to band gap, both U=4eV J=0eV and U=3eV J=0eV are within the range of reported experimental values. However, from the values for the magnetic moment, the U=4eV J=0eV case is the closest to the experimentally reported value.

U (eV)	J (eV)	Band Gap (eV)	Magnetic Moment (μ_B)
1	0	0.67	2.60
2	0	0.78	2.67
3	0	2.31	2.69
3	1	1.48	
4	0	1.90	2.81
Experiment[39,40]		2.1 ± 0.2	3.33

Table 2 Band gaps and magnetic moments for the best candidate for all values of U and J considered for $KCoF_3$.

To show that FA can find these states, as well as any metastable states, the searcher must satisfy the following:

1. The lowest-energy candidate improves as the generation number increases.

2. The diversity of candidates increases as the generation number increases.

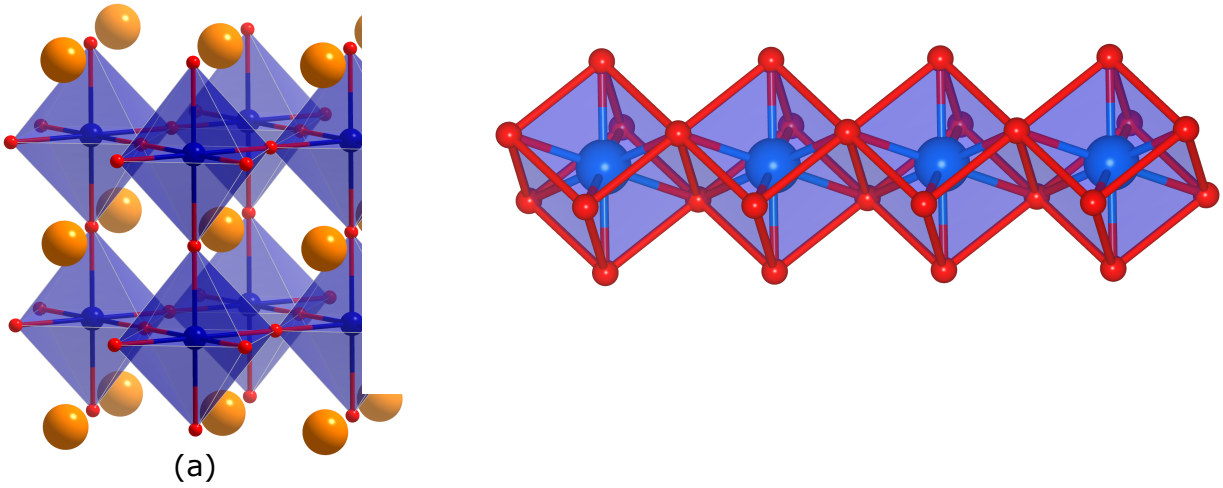

Fig. 1 Cells used for each calculation. (a) $KCoF_3$. Octahedra are shown in blue. (b) UO_2.

While the use of any metaheuristic can never guarantee that the lowest-energy solution is the ground state, it should at the very least approximate it or approach it. Improvement of the lowest-energy candidate as the searcher explores more of the PES is a necessary criterion for this. In addition, as the searcher evolves (meaning that the total number of generations is increasing), the area of the PES which it explores also increases. This means that the total diversity of candidates should also increase. To show the first point, the energy differences between the low-energy candidate of each generation and the best candidate can be plotted as a function of the generation number, as we show in Figure 2.

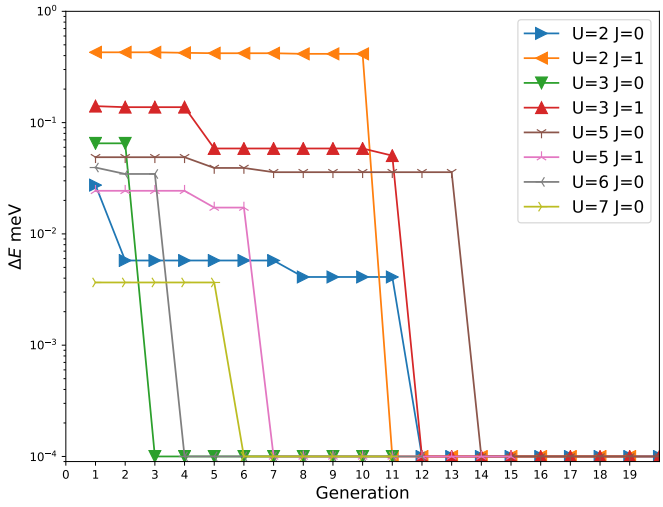

Fig. 2 Differences in energy of the best candidate in each generation relative to the energy of the lowest energy candidate found. As the semilog of zero diverges, an energy difference of 10^{-4} meV was used when the search have reached the best candidate during search.

As this is a semilog plot, the best candidate cannot be shown, as the semilog of zero is undefined, and approaches infinity. To rectify this, the points corresponding to the best candidate are automatically set to 10^{-10} eV, as this is significantly lower than any order of magnitude decrease as the searcher evolves. Discounting this, it can be seen from this figure that the candidates mostly improve by two-to-three orders of magnitude. As a secondary point, the best candidate should survive for 10 generations to prove that the stabilization limit is reached. To further show improvement, the first row of Figure 3 displays the total number of unique candidates found up to a given generation. The total number tends to increase as the generation number increases, up to a point where the total number stalls. Still stalling occurs because of two reasons. The first is that the lowest-energy candidate has remained stable; no new low-energy candidate is found. The second is that the region local to the lowest-energy candidate has been adequately explored; no new candidates are found because there are no more to be found. This second point is further clarified in the second and third rows of the figure.

The second row of Figure 3 displays the distance graphically between pairs of unique candidates found after the search completes. The diagonal is dark blue, indicating that the distance between a candidate with itself is zero. The more yellow a square, the greater the distance between candidates. For the most part, the majority of the squares are a shade of yellow, showing that the distances between candidates is small. This indicates that the searcher is targeted, as it is primarily searching over local regions of the PES. This is further clarified in the third row, which displays a network plot for the unique candidates. Connected nodes are those in which the distance between the two candidates is less than 0.4 radians. This value must be chosen carefully, as selecting a tolerance which is too small will cause the plot to be totally disconnected, and selecting too large of a value will connect every node to every other node. Essentially, it must be selected so that minima which are close to one another are connected, but minima which are far are not. The total number of clusters was determined as a function of the distance cutoff. This is shown in Figure 4.

For all values of U and J, if the tolerance was set to 0.55 radians, only one cluster existed, showing the network was fully connected. This indicates that 0.55 radians is too large of a tolerance. If the tolerance was set to lower than 0.2 radians, the clustering

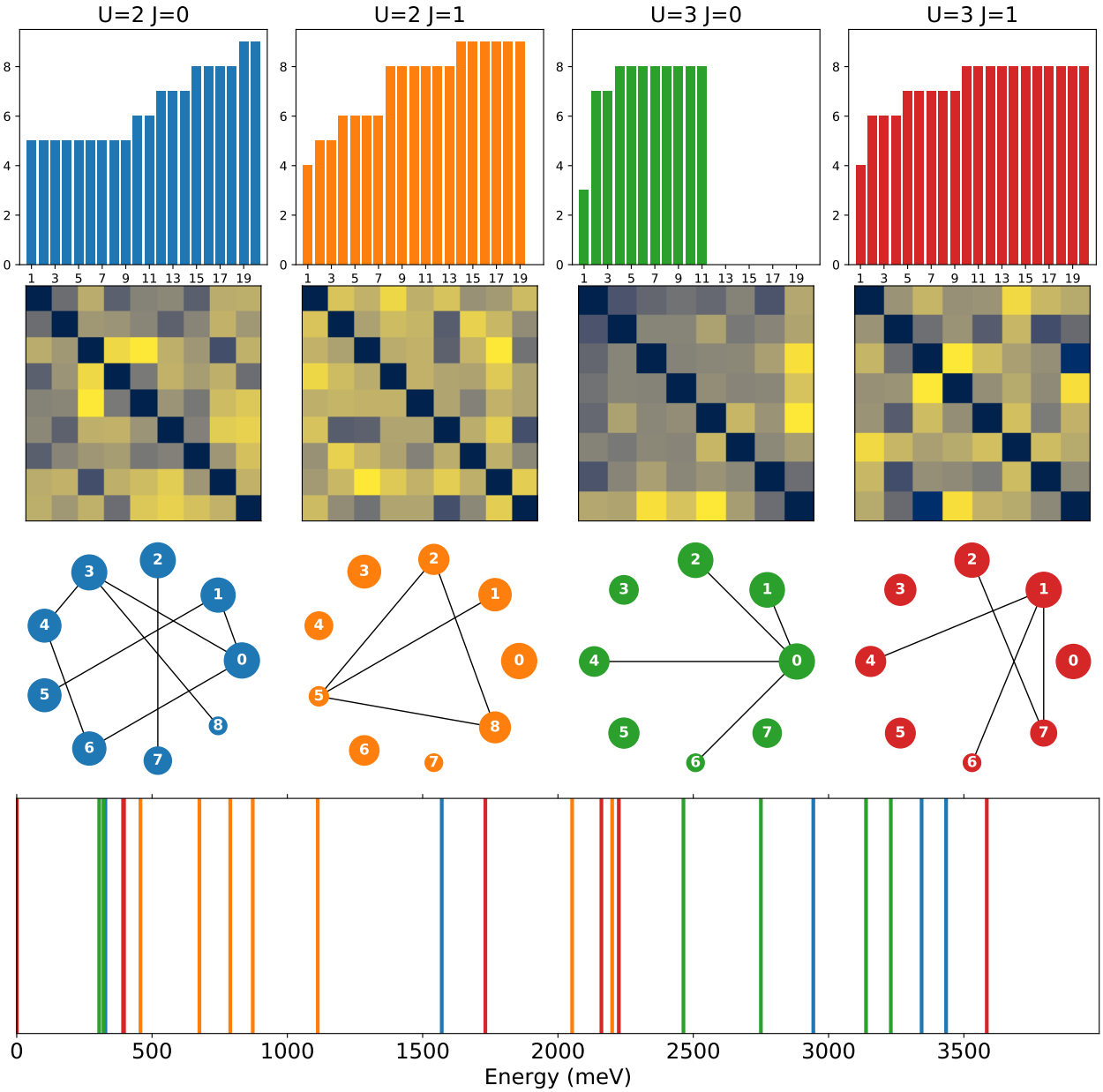

Fig. 3 Population diversity and improvement per iteration of the orbital occupation optimization for $KCoF_3$ case. Each column represents values for a particular U and J. The first row shows bars representing the cumulative number of non-equivalent candidates found up to a given number of generations. The second row shows the distance matrix for all different candidates at the end of the search. Yellow on the cell (i,j) represents candidates with very different generalized Euler angles between candidates i and j. Dark blue colors like the diagonal shows candidates with very similar Euler angles. The third row is a network representation of all different candidates found at the last iteration. Edges connecting two nodes mean that the distance value is less than 0.4. The size of each node is inversely proportional to the energy of the corresponding orbital configuration. The larger the node, lower is the energy. The last row shows the differences in energy for all candidates relative to the minimal energy found for that particular U and J.

vanishes and a totally disconnected network plot is generated. From this, 0.4 was chosen, as it strikes a balance between the two extremes. With this chosen value, a number of clustered nodes can be seen in each network plot. In addition, the larger a node is, the more energetically favorable it is. It can also be seen that the clustering primarily occurs between the lower-energy candidates. This clustering around low-energy candidates is precisely why FA is useful for orbital occupation optimization, it primarily searches in areas local to low-energy candidates on the PES. So, the search is both targeted and exploratory; it devotes candidates searching around the region which lies close to good minima, but at the same time explore random regions of the PES for potentially other competitive minima.

The lowest energy candidate for non-zero values of U and J always had the high-spin configuration $t_{2g}^5 e_g^2$, as expected for this crystal. Unsurprisingly, for U = 0 eV and J = 0 eV, the electrons are delocalized. The energy differences between all candidates in the final generation for different U and J values are displayed in the bottom panel of Figure 3. This figure also shows the large diversity of population elements as the search evolve. The orbitals for the lowest-energy candidate are displayed in Figure 5. There is a two-fold degeneracy found for the lowest-energy candidate; there are two candidates with different occupations with the same energy. While there should be three degenerate occupancies by symmetry, the failure of FA to locate all three is not a failure of the algorithm. These two-candidates appear for U $\neq$ 0. In both of these candidates, the majority spin channel has 5 electrons occupying all possible d-orbital; they differ in the minority spin channel. In one case, one electron occupies the xy orbital, the other in a linear combination of xz and xy. In the other case, one electron occupies xz while the other is in a linear combination of xy and yz. For the linear combination of orbitals, every single term has a half contribution. These are shown in Figure 5.

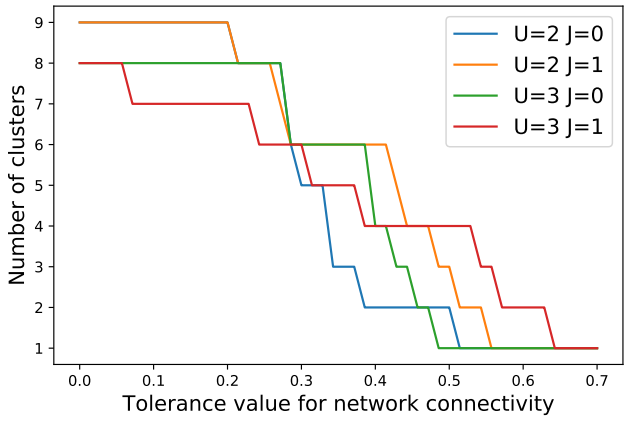

Fig. 4 Total number of clusters vs. distance tolerance for connectivity for $KCoF_3$. This distance tolerance determines how nodes are connected. If the distance between two nodes is less than this tolerance, the nodes are connected. If the distance is greater than this tolerance, they are not connected. The total number of clusters is the number of disconnected regions in the network plot. If the distance tolerance is small, then no nodes will be connected, so the total number of nodes will be equal to the total number of clusters. If the distance tolerance is too large, then all nodes are connected, so there is only one cluster. This clustering is a measure of how close minima are to one another on the PES.

Besides, the value of the magnetic exchange constants was calculated for the lowest energy candidate for all values of U and J considered. The values along several spatial directions, $J_x = \mathbf{a}+\mathbf{b}$, $J_y = -\mathbf{a}+\mathbf{b}$, and $J_z = \mathbf{c}$, are listed in Table 3.

U (eV)	J (eV)	J_x (meV)	J_y (meV)	J_z (meV)
0	0	-12.02	-11.456	-11.46
1	0	-12.75	-9.37	-11.73
2	0	-10.99	-8.24	-10.16
2	1	-8.20	-8.41	-8.41
3	0	-5.34	-3.82	-1.47
3	1	-6.36	-10.33	-10.33
4	0	-4.78	-1.31	-3.47
Experiment[37]		1.2		
Experiment[41]		4.5		

Table 3 Magnetic exchange constants for the lowest-energy candidates of $KCoF_3$. U=3eV J=0eV and U=4eV J=0eV have values within the range of those previously reported. The reported values are spatial averages.

Both U=3 eV J=0 eV and U=4 eV J= 0 eV have magnetic exchange values within the range of accepted experimental values, which are 1.2 meV to 4.5 meV.[37,41,42]. However, from our calculated values of the band gap and the magnetic exchange, U=4 eV J=0 eV is the best set of parameters to reproduce most of the experimental values together.

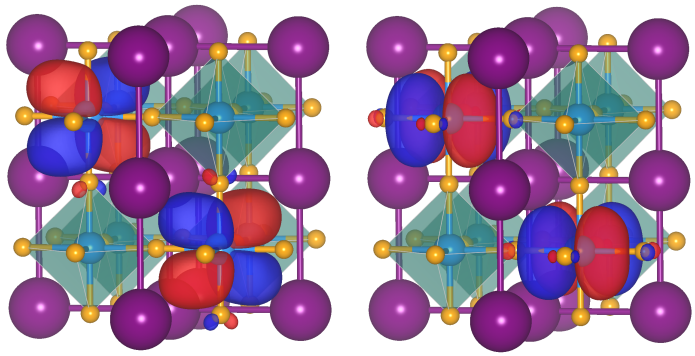

Fig. 5 Occupied orbitals of the minority spin-channel for the best candidate for U=4 eV J=0 eV. The Wannier function for a single Co is identical on each site.

4.2 UO_2

The second system chosen as a test case for our FA is *Fm-3m* uranium dioxide (UO_2). UO_2 is the standard fuel used in pressurized water nuclear reactors. Due to this, it has been extensively studied both experimentally and theoretically. Both LDA and GGA predict that UO_2 is a metallic ferromagnetic, but it is known experimentally to be an antiferromagnetic Mott insulator[43]. While UO_2 has been shown from both experiment and calculation[44,45] to have 3**K** antiferromagnetic (AFM) order, we have assumed 1**K** AFM order, as the uranium atom's spins change sign along the z-axis. This changes the point symmetry group of UO_2 from O_h to D_{4h}. The crystal field then splits the 5f orbitals of uranium into two two-fold degenerate levels, E_u, and three non-degenerate levels, A_{2u}, B_{1u}, and B_{2u}. In UO_2, only two electrons are in the 5_f

shell, so the initial diagonal matrix from which all other candidates are generated will have a trace equal to two. We start with the primitive cell for UO_2, and note that it only contains one uranium atom. The cell parameters for the primitive cell are $a = b = c = 3.83$Å, and its Wyckoff positions are listed in Table 4. Since there is only one uranium atom in the primitive cell, a supercell must be constructed from the primitive cell in order to capture the AFM nature of UO_2. We use a 4x1x1 supercell and this is used for all calculations. The supercell is displayed in Figure 1.

UO_2 *Fm-3m*

Atom	Wyckoff Position	x	y	z
U1	4b	0.50	0.50	0.50
O1	8c	0.75	0.75	0.75

Table 4 Structural information for UO_2. Coordinates for each atom are in reduced coordinates.

As in the case of $KCoF_3$, we wish to show that the lowest-energy candidate converges with respect to the generation number, and that the PES is adequately explored. Unlike in the case of $KCoF_3$, there are several computational studies[46,47] which have been performed to determine the orbital occupations of the ground state of UO_2, so our results can be directly compared to previous studies. As a word of caution, however, in each of these studies, the methods used are not exhaustive, and it is emphasized that there was no guarantee that the full orbital occupation space is explored.

In the work performed by Dorado *et. al.*[47], the occupation matrix control method was used to find the lowest energy state in UO_2 with fluorite-structure with a twelve atom cell. They also presumed 1**K** AFM ordering. With the presumption of no symmetry (therefore allowing the cubic symmetry to be broken), they found two degenerate low-energy states and ten metastable states. Using values $U = 4.50$ eV and $J = 0.51$ eV, Dorado *et. al.* relaxed UO_2 to the ground state when the occupancy matrices were initially imposed to have integer occupancy for the m=-1, m=0 or the m=0, m=1 orbitals. These initially defined occupation matrices are then relaxed. These two cases had band gaps which were comparable to the experimentally reported value of 2 eV. However, as previously stated, it is not guaranteed that this corresponds to the true ground state. This is emphasized by the energy differences found between the lowest energy state and the next highest energy state, which differed only by 0.02 eV.

This makes UO_2 an ideal complex test case for our FA implementation to explore the multiple f-orbital occupation minima. As previously shown for $KCoF_3$, it must be shown that the lowest-energy candidate improves in each subsequent generation and a significant area of the PES is explored. Unlike the previously cited work, we use combinations of U=2,3,4 and 5 eV with J=1 and 2 eV, with $U > J$.

In Figure 6 we show the convergence of the lowest-energy candidate found with respect to the generation for all values of U and J considered for UO_2. Just as with $KCoF_3$, the lowest-energy candidate improves by 2-3 orders of magnitude. Additionally, the total number of unique candidates found up to a given generation is displayed in Figure 7. Just as with $KCoF_3$, the total number increases until the search has explored all minima local to the low-energy candidates.

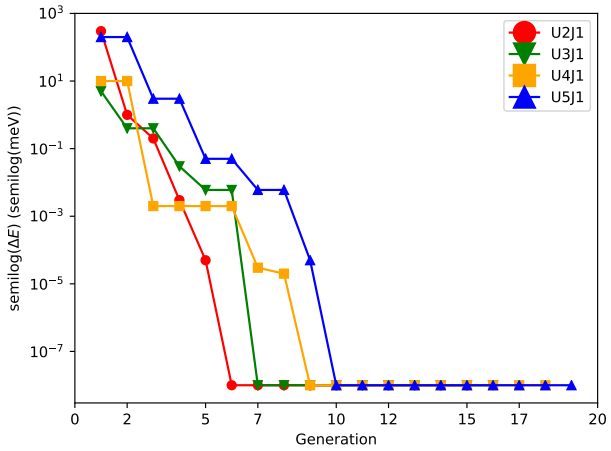

Fig. 6 Semilog plot of the energy of the best candidate in each generation relative to the energy of the lowest energy candidate found for all values of U and J considered for UO_2. As the semilog of zero diverges, an energy difference of 10^{-8} meV was used for candidates which have the same energy as this candidate, as this value of energy is at least two orders of magnitude lower than the energy difference between any candidate with this lowest energy candidate.

Using the same distance cutoff as with $KCoF_3$, we see that the unique candidates lie closer to one another from the distance plot in the second row of Figure 7. In addition, the network plot in the third row of this figure is even more connected than $KCoF_3$. This indicates that the candidates for UO_2 lie very close to one another on the PES. Just as before, this is precisely why FA is useful to the problem of orbital occupation optimization, as it allows for efficient exploration over local regions of the PES.

For all values of U and J considered, all of the metastable states previously reported were located by FA. Furthermore, since the search is performed over several different pairs of values, the low-energy states can be compared across the selected values of U and J. For the values of U and J considered, the low-energy state found by FA has a different occupation than what is reported previously. This indicates that for UO_2 the particular orbitals occupied depends on the choice of U and J. Unlike $KCoF_3$, UO_2 shows that the variations in the occupied orbitals differ across the different values of U considered. The variation of the occupancy across U for J= 1 eV is shown in Figure 8. For the values of U and J which are the most similar to Dorado *et. al.*, which in their case are U=4.5, J=0.51, we find for U=4 eV J=1 eV that the two electrons occupy f_{yz^2} and a linear combination of $f_{z(x^2-y^2)}$ and f_{xyz}. The orbitals for this low-energy configuration are displayed in Figure 9 In comparison, the ground state found by Dorado *et. al.* was $f_{z(x^2-y^2)}$ and a linear combination of $f_{x(x^2-3y^2)}$ and $f_{z^3)}$. However, care must be taken here as the values of U and J are not identical, and we have found that the low-energy occupation for UO_2 is sensitive to the choice of U and J (Figure 8). In their work, this state was found when non-diagonal occupation matrices were considered and is 0.02 eV lower in energy than the ground state found when only integer occupations were considered. We are also able

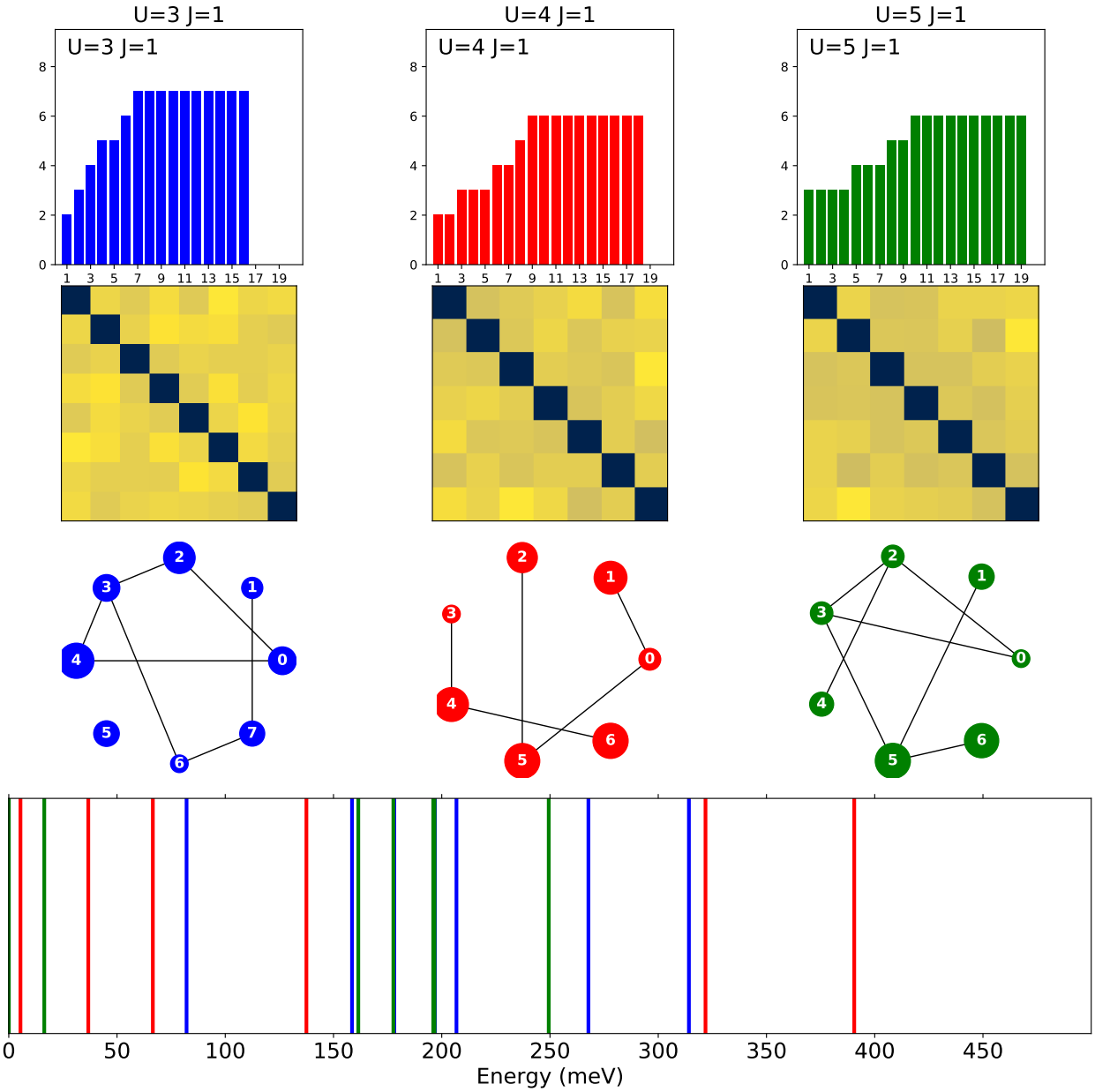

Fig. 7 Population diversity and improvement per iteration of the orbital occupation optimization for UO_2 case. Each column represents values for a particular U and J. The first row shows bars representing the cumulative number of non-equivalent candidates found up to a given number of generations. The second row shows the distance matrix for all different candidates at the end of the search. Yellow on the cell (i,j) represents candidates with very different generalized Euler angles between candidates i and j. Dark blue colors like the diagonal shows candidates with very similar Euler angles. The third row is a network representation of all different candidates found at the last iteration. Edges connecting two nodes mean that the distance value is less than 0.4. The size of each node is inversely proportional to the energy of the corresponding orbital configuration. The larger the node, lower is the energy. The last row shows the differences in energy for all candidates relative to the minimal energy found for that particular U and J.

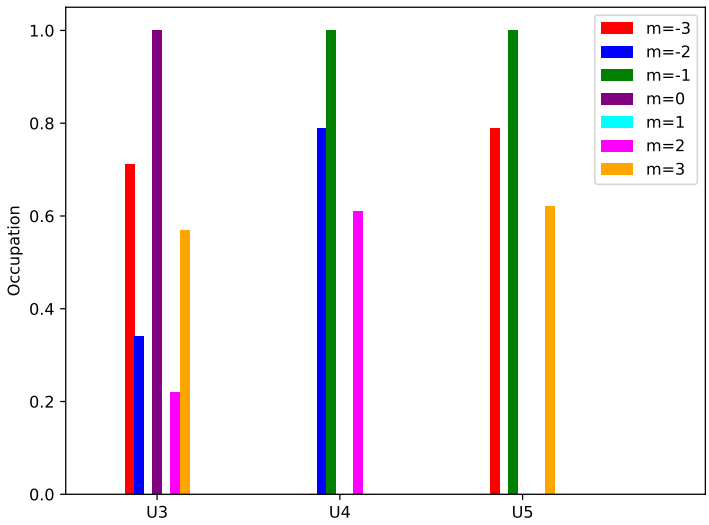

Fig. 8 Orbital occupations of the ground states obtained for UO_2 for $U =$ 3, 4 and 5 eV with J=1 eV.

to find their reported low-energy state when integer occupations were enforced, with the two electrons occupying f_{xyz} and f_{xz^2}, and similarly, it is one of the metastable states found with FA. For U= 4 eV, J = 1 eV, this state is 1.98 eV higher in energy than the low-energy state found with FA, indicating that our low-energy state is even lower in energy than that previously reported, which proves that using a metaheuristic search of occupation matrices could be more powerful than "hand-made" techniques.

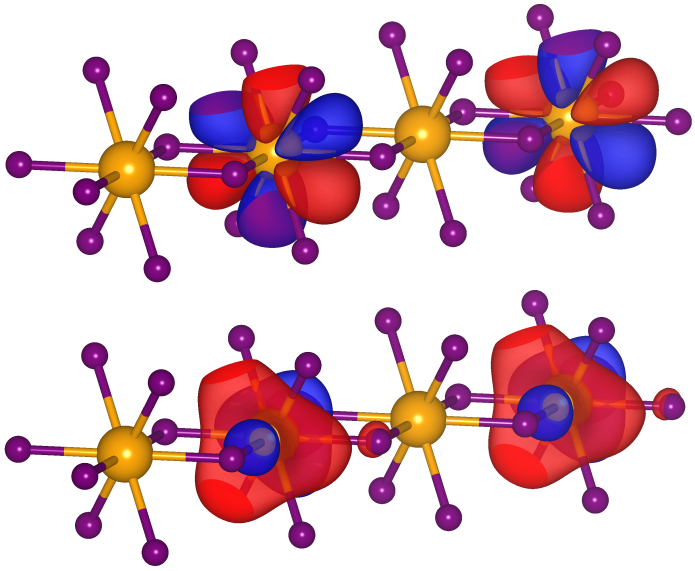

Fig. 9 Occupied orbitals for the best candidate for U=4 eV J=1 eV. The Wannier functions are identical on each U site.

5 Conclusion

In this paper, we have demonstrated that the firefly algorithm is a powerful technique to explore multiple regions of orbital occupation PES in the d-electron and f-electron systems. Since multiple regions are simultaneously probed, a multitude of stable orbital configurations can be obtained quickly. The method does not depend on specific details of the system other than the particular orbitals which are being corrected, which also means that any DFT code that can constrain the occupation matrix can be used. The efficiency of the method coupled with its independence with respect to system-dependent details, makes FA well-suited to the problem of locating possible stable orbital configurations.

We have tested our implementation on two examples: the perovskite $KCoF_3$ with d-orbitals and UO_2 with f-electrons where in both cases the FA was able to identify a multitude of metastable states with different occupations and to identify the lowest energy one among the series. Moreover, the method itself could be used to sweep over many values of U and J to locate the values which yield an occupancy which is in agreement with experiment. This method improves upon the currently used brute-force methods in which the ground state is found through changing the initial occupation matrix by hand. At the same time, it can be used in conjunction to the optimization of magnetic orientation in non-collinear calculations, by interfacing this methodology with the one reported in Ref[20] The method could be also very important for hybrid functionals, which have the same problem of multiple minima in the orbital occupations. The addition of spin-orbit coupling could worsen the problem and such metaheuristic methods could be handful to identify the lowest energy occupations of non-collinear magnets.[20].

We hope our method to be helpful in many systems with strongly correlated electrons where multiple minima occupations make their study difficult for DFT calculations.

Conflicts of interest

There are no conflicts of interest to declare.

Acknowledgments

The authors thank Bernard Amadon for useful discussions. This work used the XSEDE which is supported by National Science Foundation grant number ACI-1053575. XH and EB acknowledge the ARC project AIMED and the F.R.S-FNRS PDR project MaRePeThe (GA 19528980). The authors also acknowledge the computational support from the Texas Advanced Computer Center (TACC) (for Stampede2) and Pittsburgh Supercomputing Center (PSC) (for Bridges), the PRACE project TheDeNoMo, the CECI facilities funded by F.R.S-FNRS (Grant No. 2.5020.1) and Tier-1 supercomputer of the Fédération Wallonie-Bruxelles funded by the Walloon Region (Grant No. 1117545). Calculations were performed on Spruce Knob and Thorny Flat, supercomputers at West Virginia University, which were funded in part by the National Science Foundation (NSF) Major Research Instrumentation Program (MRI) Award #1726534. This work was supported by the DMREF-NSF 1434897, NSF OAC-1740111 and DOE DE-SC0016176 projects.

Notes and references

1 A. J. Cohen, P. Mori-Sánchez and W. Yang, *The Journal of Chemical Physics*, 2008, **129**, 121104.

2 A. J. Cohen, P. Mori-Sánchez and W. Yang, *Science*, 2008, **321**, 792–794.

3 J. P. Perdew and A. Zunger, *Phys. Rev. B*, 1981, **23**, 5048–5079.

4 A. Filippetti and N. A. Spaldin, *Phys. Rev. B*, 2003, **67**, 125109.

5 M. Cococcioni, in *Correlated Electrons: From Models to Materials Modeling and Simulation*, ed. E. Pavarini, E. Koch, A. Frithjof and M. Jarrell, 2012, ch. The LDA + U Approach : A Simple Hubbard Correction for Correlated Ground States.

6 D.-K. Seo, *Phys. Rev. B*, 2007, **76**, 033102.

7 V. I. Anisimov, F. Aryasetiawan and A. I. Lichtenstein, *Journal of Physics: Condensed Matter*, 1997, **9**, 767–808.

8 S. Grimme, *The Journal of Chemical Physics*, 2006, **124**, 034108.

9 F. Tran, P. Blaha, K. Schwarz and P. Novák, *Phys. Rev. B*, 2006, **74**, 155108.

10 V. I. Anisimov, A. I. Poteryaev, M. A. Korotin, A. O. Anokhin and G. Kotliar, *Journal of Physics: Condensed Matter*, 1997, **9**, 7359–7367.

11 G. Kotliar, S. Y. Savrasov, K. Haule, V. S. Oudovenko, O. Parcollet and C. A. Marianetti, *Rev. Mod. Phys.*, 2006, **78**, 865–951.

12 A. Georges, G. Kotliar, W. Krauth and M. J. Rozenberg, *Rev. Mod. Phys.*, 1996, **68**, 13–125.

13 H. Park, A. J. Millis and C. A. Marianetti, *Physical Review B*, 2014, **90**, 235103.

14 P. Larson, W. R. L. Lambrecht, A. Chantis and M. van Schilfgaarde, *Phys. Rev. B*, 2007, **75**, 045114.

15 B. Dorado, B. Amadon, M. Freyss and M. Bertolus, *Phys. Rev. B*, 2009, **79**, 235125.

16 G. Jomard, B. Amadon, F. Bottin and M. Torrent, *Phys. Rev. B*, 2008, **78**, 075125.

17 B. Amadon, F. Jollet and M. Torrent, *Phys. Rev. B*, 2008, **77**, 155104.

18 H. Y. Geng, Y. Chen, Y. Kaneta, M. Kinoshita and Q. Wu, *Phys. Rev. B*, 2010, **82**, 094106.

19 G. Avendaño Franco and A. H. Romero, *Journal of Chemical Theory and Computation*, 2016, **12**, 3416–3428.

20 A. Payne, G. Avendaño Franco, E. Bousquet and A. H. Romero, *Journal of Chemical Theory and Computation*, 2018, **14**, 4455–4466.

21 D. K. Hoffman, R. C. Raffenetti and K. Ruedenberg, *Journal of Mathematical Physics*, 1972, **13**, 528–533.

22 X. Gonze, B. Amadon, P.-M. Anglade, J.-M. Beuken, F. Bottin, P. Boulanger, F. Bruneval, D. Caliste, R. Caracas, M. Côté, T. Deutsch, L. Genovese, P. Ghosez, M. Giantomassi, S. Goedecker, D. Hamann, P. Hermet, F. Jollet, G. Jomard, S. Leroux, M. Mancini, S. Mazevet, M. Oliveira, G. Onida, Y. Pouillon, T. Rangel, G.-M. Rignanese, D. Sangalli, R. Shaltaf, M. Torrent, M. Verstraete, G. Zerah and J. Zwanziger, *Computer Physics Communications*, 2009, **180**, 2582 – 2615.

23 X. Gonze, G. Rignanese, M. Verstraete, J. Betiken, Y. Pouillon, R. Caracas, F. Jollet, M. Torrent, G. Zerah, M. Mikami, P. Ghosez, M. Veithen, J.-Y. Raty, V. Olevano, F. Bruneval, L. Reining, R. Godby, G. Onida, D. Hamann and D. Allan, *Zeitschrift für Kristallographie.(Special issue on Computational Crystallography.)*, 2005, **220**, 558–562.

24 X. Gonze, J.-M. Beuken, R. Caracas, F. Detraux, M. Fuchs, G.-M. Rignanese, L. Sindic, M. Verstraete, G. Zerah, F. Jollet, M. Torrent, A. Roy, M. Mikami, P. Ghosez, J.-Y. Raty and D. Allan, *Computational Materials Science*, 2002, **25**, 478 – 492.

25 M. Torrent, F. Jollet, F. Bottin, G. Zérah and X. Gonze, *Computational Materials Science*, 2008, **42**, 337 – 351.

26 X. Gonze, F. Jollet, F. A. Araujo, D. Adams, B. Amadon, T. Applencourt, C. Audouze, J.-M. Beuken, J. Bieder, A. Bokhanchuk *et al.*, *Computer Physics Communications*, 2016, **205**, 106–131.

27 J. P. Perdew, *International Journal of Quantum Chemistry*, 1985, **28**, 497–523.

28 M. van Setten, M. Giantomassi, E. Bousquet, M. Verstraete, D. Hamann, X. Gonze and G.-M. Rignanese, *Computer Physics Communications*, 2018, **226**, 39 – 54.

29 F. Jollet, M. Torrent and N. Holzwarth, *Computer Physics Communications*, 2014, **185**, 1246 – 1254.

30 V. I. Anisimov and O. Gunnarsson, *Phys. Rev. B*, 1991, **43**, 7570–7574.

31 A. I. Liechtenstein, V. I. Anisimov and J. Zaanen, *Phys. Rev. B*, 1995, **52**, R5467–R5470.

32 *PyChemia*, `https://github.com/MaterialsDiscovery/PyChemia`.

33 A. Liechtenstein, M. Katsnelson, V. Antropov and V. Gubanov, *Journal of Magnetism and Magnetic Materials*, 1987, **67**, 65 – 74.

34 A. A. Mostofi, J. R. Yates, G. Pizzi, Y.-S. Lee, I. Souza, D. Vanderbilt and N. Marzari, *Computer Physics Communications*, 2014, **185**, 2309 – 2310.

35 D. M. Korotin, V. V. Mazurenko, V. I. Anisimov and S. V. Streltsov, *Phys. Rev. B*, 2015, **91**, 224405.

36 K. Knox, *Acta Crystallographica*, 1961, **14**, 583–585.

37 T. M. Holden, W. J. L. Buyers, E. C. Svensson, R. A. Cowley, M. T. Hutchings, D. Hukin and R. W. H. Stevenson, *Journal of Physics C: Solid State Physics*, 1971, **4**, 2127–2138.

38 A. Jain, S. P. Ong, G. Hautier, W. Chen, W. D. Richards, S. Dacek, S. Cholia, D. Gunter, D. Skinner, G. Ceder and K. a. Persson, *APL Materials*, 2013, **1**, 011002.

39 G. Pari, S. Mathi Jaya and R. Asokamani, *Phys. Rev. B*, 1994, **50**, 8166–8169.

40 V. Manivannan, P. Parhi and J. W. Kramer, *Bulletin of Materials Science*, 2008, **31**, 987–993.

41 D. Breed, K. Gilijamse and A. Miedema, *Physica*, 1969, **45**, 205 – 216.

42 T. Onishi and Y. Yoshioka, *e-Journal of Surface Science and Nanotechnology*, 2007, **5**, 17–19.

43 S.-W. Yu, J. G. Tobin, J. C. Crowhurst, S. Sharma, J. K. Dewhurst, P. Olalde-Velasco, W. L. Yang and W. J. Siekhaus, *Phys. Rev. B*, 2011, **83**, 165102.

44 R. Caciuffo, G. Amoretti, P. Santini, G. H. Lander, J. Kulda and

P. d. V. Du Plessis, *Phys. Rev. B*, 1999, **59**, 13892–13900.
45 A. M. Chaka, G. A. Oxford, J. E. Stubbs, P. J. Eng and J. R. Bargar, *Computational and Theoretical Chemistry*, 2012, **987**, 90 – 102.
46 J. P. Allen and G. W. Watson, *Phys. Chem. Chem. Phys.*, 2014, **16**, 21016–21031.
47 B. Dorado, G. Jomard, M. Freyss and M. Bertolus, *Phys. Rev. B*, 2010, **82**, 035114.